

# Fractal noise maps reveal human brain activity: a key for unbiased fMRI analysis

Stefan Thurner<sup>1¶¶¶</sup>, Christian Windischberger<sup>2</sup>,  
Ewald Moser<sup>2</sup>, Markus Barth<sup>2</sup>

<sup>1</sup>*Institut für Mathematik NuHAG and Universitätsklinik für HNO,*

<sup>2</sup>*Universitätsklinik für Radiodiagnostik,*

*University of Vienna; Währinger Gürtel 18-20; A-1090 Vienna; Austria*

(Dated: August 2002)

## Abstract

Brain metabolism is controlled by complex regulation mechanisms. As part of their nature many complex systems show scaling behavior in their timeseries data. Corresponding scaling exponents can sometimes be used to characterize these systems. Here we present maps of scaling exponents derived from BOLD functional Magnetic Resonance Imaging (fMRI) data, and show that they reveal activation patterns in the human brain with very high precision. In contrast to standard model-based analysis we use no prior knowledge on the experimental stimulation paradigm for extracting activation patterns from fMRI timeseries. We demonstrate that mental activity is one-to-one related to large fractal exponents, or equivalently, to temporally highly correlated processes.

PACS: 87.10.+e, 87.57.-s, 87.61.-c, 05.45.Df, 05.45.Tp

---

### ¶¶¶ Correspondence to:

Prof. Stefan Thurner PhD, PhD; HNO, AKH-Wien, University of Vienna  
Währinger Gürtel 18-20; A-1090 Vienna, Austria  
Tel.: ++43 1 40400 2099; Fax: ++43 1 40400 3332  
e-mail: thurner@univie.ac.at

Functional magnetic resonance imaging (fMRI) based on Blood Oxygenation Level Dependent (BOLD) signal-changes allows assessment of brain activity via local haemodynamic variations over time [1]. It provides the highest combined spatial and temporal resolutions presently available for non-invasive functional brain mapping. In fMRI measurements slices of the human brain are sampled in a repetitive manner with  $\text{mm}^3$  sized voxels as the smallest information-carrying spatial element. These represent aggregated and collective information on the physiological status of a large number of neurons with a temporal resolution of tens of ms. In a typical fMRI experiment external (e.g. visual) stimuli are presented in intervals of several seconds ( $\sim 0.1$  Hz), causing a change in voxel-signal intensity, delayed and blurred by the haemodynamic response [2, 3]. Functional MRI voxel-timeseries exhibit considerable noise components which adversely effect conventional fMRI analysis and therefore are typically considered undesired and interfering. On the other hand, by studying fMRI noise evidence has been found that voxel-timeseries potentially exhibit  $1/f$  noise characteristics [4, 5].  $1/f$  noise – e.g. characterized by a power-law decay of the Power Spectrum Density (*PSD*) – has been discovered in a wide variety of systems which are governed by complex physiological regulation mechanisms such as the cardiovascular system [6, 7].

Brain metabolism is controlled by a variety of complex mechanisms that guarantee proper brain function including sufficient blood supply to meet neural demands. Increased metabolic demand is triggered by mental processes and initiates a cascade of biochemical reactions, followed by changes in haemodynamic parameters such as blood flow and oxygenation [8]. In this work we argue that the use of high temporal-resolution BOLD fMRI in combination with a scaling analysis enables us to distinguish different physiological states (active and non-active) of the brain. We show that this is a robust method and can be seen already by using relatively simple fractal noise-measures like Hurst- and *PSD*-exponents. We focus on the statistical scaling structure of voxel-timeseries obtained in fMRI experiments and visualize the amount of information present in the “noise”.

Noise structure can be characterized by so-called fractal measures. Usually one uses more than one method to avoid well known systematic deficiencies inherent to either method [9]. Here we use two of the simplest methods available.

*Hurst Exponent:* The concept of Brownian motion (random walk) can be generalized to fractional Brownian motion [10] by introducing a scaling exponent  $H$ , often called Hurst exponent. Maybe the most transparent way to define it is by the two-point correlation

function of a (stochastic) data timeseries  $x(t)$ ,

$$C(\tau) = \langle [x(t + \tau) - x(t)]^2 \rangle \propto \tau^{2H} \quad , \quad (1)$$

with  $H$  being a real number,  $0 < H < 1$ .  $H$  serves to characterize the process in terms of temporal correlations: while for classical Brownian motion ( $H = 0.5$ ) there are no correlations, for  $H > 0.5$  the process is called positively correlated or persistent, i.e., if the process was moving upward (downward) at time  $t$  it will tend to continue to move upward (downward) at future times  $t' > t$  as well. This means that increasing (decreasing) trends in the past imply – on average – increasing (decreasing) trends in the future [11]. If  $H < 0.5$  the corresponding process is called anti-correlated or anti-persistent, meaning that increasing (decreasing) trends in the past imply – on average – decreasing (increasing) trends.

*Power-Spectrum exponent:* Alternatively, one can quantify internal noise structure in stochastic processes by the power-spectrum exponent  $S$ , defined by the power characterizing the decay of the (discrete) *PSD*, i.e., the squared Fourier spectrum of the process  $x(t)$ ,

$$PSD(\omega) = \left| \sum_{k=1}^N x(k) e^{i2\pi(\omega-1)(k-1)/N} \right|^2 \propto \omega^{-S} \quad , \quad (2)$$

with  $N$  being data size. For perfect 1-dimensional fractal processes it can be shown that  $H$  and  $S$  are related by  $S = 2H + 1$ . Hence, exponents  $H$  ( $S$ ) different from a value of 0.5 (2) indicate a self affine, internal structure of the timeseries.

Functional MRI was performed on a 3 Tesla whole-body MR scanner (MedSpec S300, Bruker, Ettlingen, Germany) using single-shot gradient echo-planar imaging (EPI), with a  $T_R$  of 200 ms and an effective  $T_E$  of 28 ms. Four 4 mm thick slices parallel to the calcarine sulcus were measured using a field-of-view of  $29 \times 29 \text{ cm}^2$  and a matrix size of  $64 \times 64$  pixels. This setup was repeated 1500 times resulting in a total measurement time of 5 minutes. A visual stimulation paradigm was presented at randomly distributed time points during scanning, separated by an interval of at least 10 seconds, guaranteeing that all stimulation frequencies are below 0.1 Hz. Stimulation consisted in presenting a rotating checker-board disk to the subjects for three seconds via video projector and mirror.

Voxel time-course information  $\bar{I}(\vec{x}, t)$  was obtained from images taken at time instances  $t$  ( $\vec{x}$  is voxel-position in 3D space). For further analysis we subtracted the temporal mean from  $\bar{I}(\vec{x}, t)$  to obtain the process  $I(\vec{x}, t) = \bar{I}(\vec{x}, t) - \langle \bar{I}(\vec{x}, t) \rangle_t$ . This process serves as the starting point for all further analysis, no more pre-processing steps, neither filtering, normalization,

nor motion correction were applied to the data. For fractal analysis we use the cumulative voxel-intensity process  $x(\vec{x}, t) = \sum_{i=1}^t I(\vec{x}, i)$ .

Standard fMRI analysis of the data sets was performed using linear regression, based on the known stimulation paradigm convolved with a model haemodynamic response function, resulting in a model function  $HR(t)$  [12]. The results of this analysis are r-maps, i.e. correlation coefficients of the model function  $HR(t)$  with actual fMRI data for all individual pixels at positions  $\vec{x}$ . Results are thresholded to reveal the pixels activated during visual stimulation. In the following a t-threshold of 5 was chosen which corresponds to a Bonferroni-corrected  $p$ -value of 0.001, representing highly significant activation.

Fig. 1 displays the averaged time-course of all activated pixels of a single, 4-slice experiment as found by standard regression analysis [13]. The corresponding functional r-maps in Fig. 2a clearly show the expected functional activation in the primary visual areas. The respective time-course is in excellent agreement with the stimulus applied, as indicated by the red bars in Fig. 1. In Fig. 2b and c, maps of  $H$  and  $S$  values are shown for all voxels within the brain slices, respectively. The color table is the same for all three parameters, however, adjusted to match the respective range of values. Regions with a large Hurst-value (red) coincide with areas of visual activation, as detected by the regression analysis with high statistical significance ( $p < 0.001$ ). The same regions can be found in the  $S$ -maps, however, to somewhat less spatial precision. Signals in frontal regions are caused by movement artifacts. We checked this by confirming that they reduce when applying standard realignment software.

To demonstrate that the observed changes in the scaling parameters  $H$  and  $S$  are in fact properties of noise, we performed the following checks: (i) *Residual analysis*: We pixel-wise fitted our data to results of the model function  $HR(\vec{x}, t)$  obtained from a linear standard fMRI model [12, 13],

$$\bar{I}(\vec{x}, t) = HR(\vec{x}, t) + \xi(\vec{x}, t) \quad , \quad (3)$$

where  $\bar{I}(\vec{x}, t)$  is the fMRI signal and  $\xi(\vec{x}, t)$  the residual noise at pixel position  $\vec{x}$ . We performed the same scaling exponent analysis as before starting from the residual dataset  $\xi(\vec{x}, t)$ . As expected the correlation coefficients become vanishingly small and can not serve as a reliable measure anymore, Fig. 3a. With  $\xi(\vec{x}, t)$  as the input,  $H$  and  $S$  are shown in Fig. 3b and c. The same areas of activity are recovered. This is a clear sign that  $\xi(\vec{x}, t)$  which is

often (wrongly) considered "white noise" still carries relevant information. One could argue here that if this is the case the model is not yet good enough and has to be improved before discussing statistical significance of activation patterns. However, actually used models are based on linear approaches and can not account for the scaling effects reported here. *(ii) Low pass filtering:* By applying successive temporal smoothing of the pixel timeseries we find that the scaling effects eventually disappear, and obviously the structure observed here is a characteristics of the noise and not of the low frequency stimulation (signal). *(iii) Background noise is white:* We find that the background noise (measurement or machine errors) in the signal as observed outside the head fluctuates around  $H = 0.5$  (mean and standard deviation:  $H = 0.492 \pm 0.046$ ), as expected.

In Fig. 4 the timeseries  $I(\vec{x}, t)$  for two selected voxels are shown, identified as either non-activated (a) or activated (b) in the standard fMRI analysis. Periods of visual stimulation are again marked with red bars. Clearly, the voxel in the visual region follows the stimulus (much like the entire cluster; compare Fig. 1). In Fig. 4c and d we show the *PSD* of  $x(\vec{x}, t)$ . Voxel timeseries show typical  $1/f$  noise characteristics and the power spectral density exponent  $S$  can be estimated safely by fits to the *PSD*-slope in a log-log plot. Fits are given by red lines. In order to focus exclusively on the noise structure and to exclude any influence of the BOLD response itself, the frequency range corresponding to the stimulus presentation (between 0.04 - 0.1 Hz) was excluded from the fit-range. Frequency fluctuations larger than 1 Hz were also not included as those frequencies are above the fractal onset frequency for the given data size [9]. In Fig. 4e and f we plot  $C(\tau)$  from Eq. 1, and extract the Hurst exponent  $H$  as half of the slope of the linear fit. Again, the same effective fit-range (red lines) was used.

A priori, noise components above the characteristic stimulus frequencies could be thought to appear as measurement noise and undesirable artifacts. In this work we have examined these noise components from a scaling point of view. We found that in non-active cortical regions, voxel-activity is well described by classical Brownian motion (random walk model,  $H \sim 0.5$  and  $S \sim 2$ ), while noise components from voxels of active brain regions – besides obviously following the stimulus – change their character towards highly correlated stochastic processes, i.e., correlated fractional Brownian noise. We have also observed that the latter regions are detected by  $H$  and  $S$  at very high sensitivity, i.e., regions of large  $H$  and closely correlate with large r-values from model-based regression analysis. In areas outside the

subject's head,  $H$  is fluctuating around 0.5 ensuring that no internal noise structure is arising or due to measurement or machine noise. These findings clearly demonstrate persistent fractal dominance of noise in voxel-timeseries in regions of neural activation, while in other areas uncorrelated noise prevails, consistent with recent work [14, 15, 16].  $S$  and  $H$  seem to be related to some extent, indicating the voxel-processes to be close to perfect fractals.

We find that even residual timeseries, as e.g. obtained by SPM software [13], show practically the same scaling information content. This finding has far reaching consequences for statistical analyses of fMRI data. Standard statistics is based on models which leave white noise as a residuum. Based on white noise, null hypotheses can be tested and sensible  $p$ -values be quoted. For correlated or scaling processes, however, it is known that standard statistics is not valid, since residua are by definition correlated (e.g. via scaling relations). As a consequence other methods based on more complicated statistics have to be used to arrive at " $p$ -values" which capture actual statistical significance. Maybe Tsallis entropy [17] and its associated non-extensive statistics offer a natural starting point for consistently solving this problem.

In conclusion we find that the statistical nature of voxel-timeseries depends on the underlying level of neural activity. In activated regions the noise processes are strongly temporally correlated. The practical potential of this study is that scaling analysis is entirely model-independent: we do not make any assumptions about the nature of the voxel-processes, but rather try to clarify it. Moreover, no information on the stimulus paradigm is required. It is intriguing that the information carried by fMRI noise alone is sufficient to at least compete with the gold-standard of fMRI analysis for detecting statistically significant regions of neural activation. Scaling measures – as a complementary source of information – may therefore improve specificity in fMRI data analysis. We believe that the use of fractal parameters in fMRI also represents a significant potential for understanding the fundamental processes involved in neuro-vascular coupling, by identifying "noise components" as valuable measurements representing detailed high(er) frequency information, rather than treating "noise" as a nuisance. Our results can be seen in the context of recent trends which focus on the practical role of noise [18], and that one should not restrict oneself to the obvious, but also hunt for the information hidden in the "noise".

- 
- [1] S. Ogawa, R.S. Menon, D.W. Tank, S.G. Kim, H. Merkle, J.M. Ellerman, K. Ugurbil, J. Biophys. **64**, 803812 (1993).
- [2] G.K. Aguirre, E. Zarahn, M. D'Esposito, NeuroImage **8**, 360-369 (1998).
- [3] C. Goutte, L.K. Hansen, M.G. Liptrop, E. Rostrup, Human Brain Mapping **13**, 165-183 (2001).
- [4] E. Zarahn, G.K. Aguirre, M. D'Esposito, NeuroImage **5**, 179-197 (1997).
- [5] S.B. Lowen, private communication.
- [6] M. Kobayashi, T. Musha, IEEE Trans. Biomed. Eng. **29**, 456-457 (1982).
- [7] R.G. Turcott, M.C. Teich, Ann. Biomed. Eng. **24**, 269-293 (1996).
- [8] N.K. Logothetis, J. Pauls, M. Augath, T. Trinath, A. Oeltermann, Nature **412**, 150-157 (2001).
- [9] S. Thurner, S.B. Lowen, M.C. Feurstein, C. Heneghan, H.G. Feichtinger, M.C. Teich, Fractals **5**, 565-595 (1997).
- [10] B.B. Mandelbrot, J.W. van Ness, SIAM Rev. **10**, 422-437 (1968).
- [11] J. Feder, *Fractals*, Plenum Press, New York (1988).
- [12] K.J. Friston, C.D. Frith, R.S. Frackowiak, R. Turner, NeuroImage **2**, 166-172 (1995).
- [13] Statistical Parametric Mapping, see homepage <http://www.fil.ion.ucl.ac.uk/spm/>
- [14] R.M. Weisskoff, J. Baker, J. Belliveau, T.L. Davis, K.K. Kwong, M.S. Cohen, and B.R. Rosen, Proceedings Int. Soc. for Magn. Reson. in Med. **1**, 7 (1993).
- [15] E. Bullmore, et al., Human Brain Mapping **12**, 61-78 (2001).
- [16] G. Krüger, G.H. Glover, Magn. Reson. Med. **46**, 631-637 (2001).
- [17] C. Tsallis, J. Stat. Phys. **52**, 479 (1988).
- [18] J.J. Collins, Nature **402**, 241 (1999).

FIG. 1: Average time-course of all activated pixels (blue line). Overlaid (red dashed line) is the functional paradigm convolved with the haemodynamic response (model function  $HR(t)$ ). The stimulation periods are indicated by red bars at the bottom.

FIG. 2: Computed “activation” maps of four brain slices using the standard linear regression analysis. Correlation coefficients (r-map) of the actual data and the functional paradigm convolved with the haemodynamic response function are shown (a). Hurst exponent analysis for the pixel timeseries (b); Power spectral exponent analysis for the pixel timeseries (c).

FIG. 3: Same as previous figure, but starting from the residual dataset  $\xi(\vec{x}, t)$ . Clearly the correlation map (a) does not show activation patterns anymore, notice the change in scale compared to the previous figure.  $H$  and  $S$  maps, (b) and (c), show the same activated regions and about the same numerical values as in the original data.

FIG. 4: Timeseries of a non-active (a) and an active (b) voxel. The power spectral exponent  $S$  for these processes is given by the slope of the  $PSD$  shown in (c) and (d). Clear  $1/f$  behavior in the  $PSD$  is observable. The Hurst exponent  $H$  is defined as half the slope of the function  $C$ .



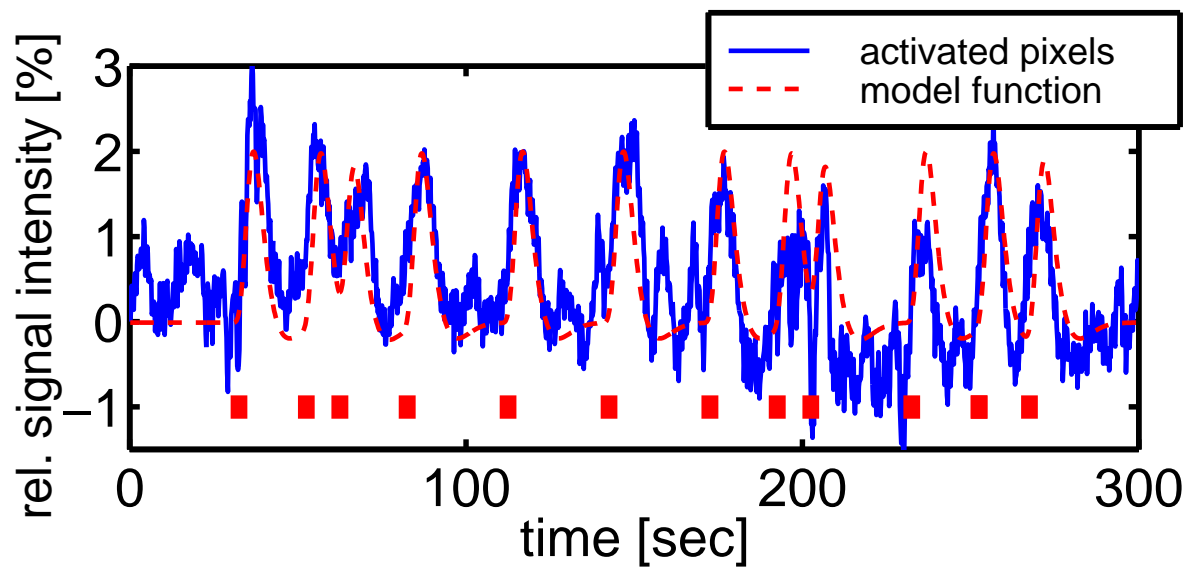
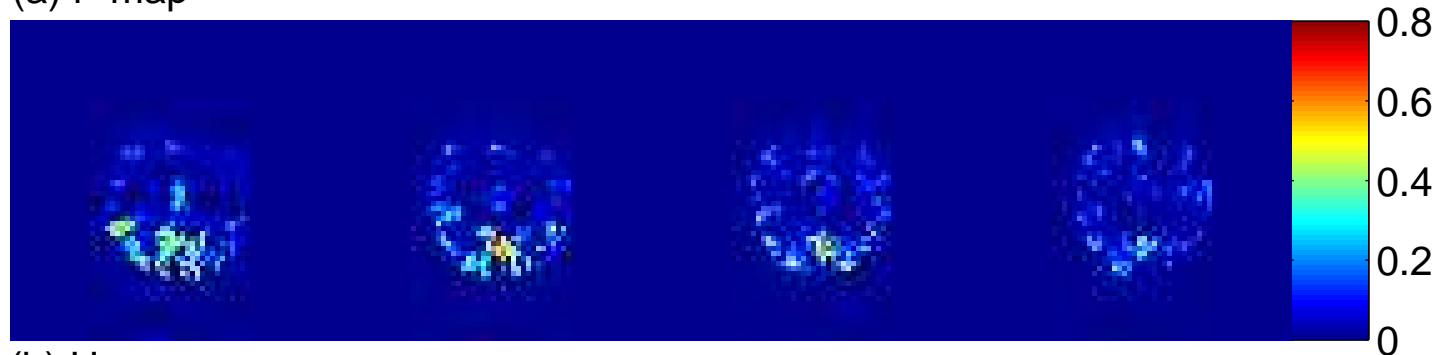
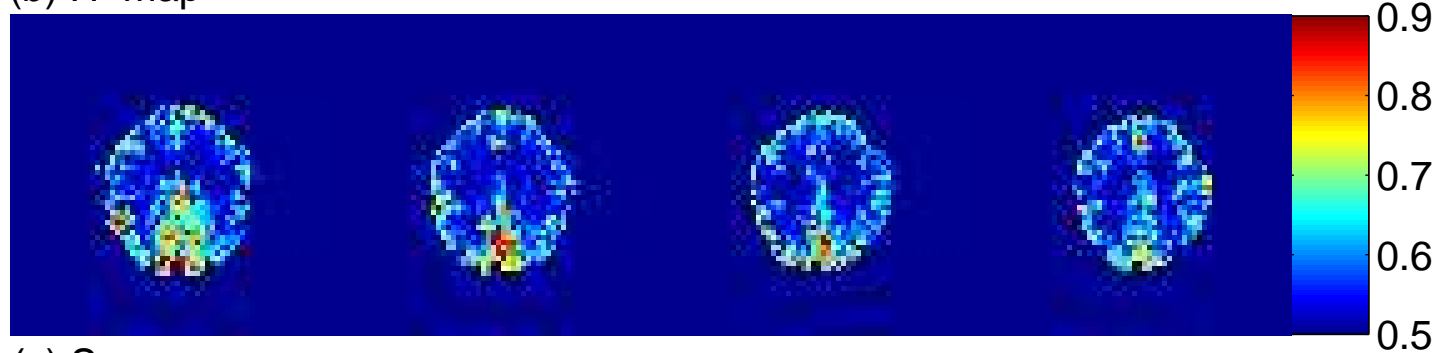


FIG. 1

(a) r-map



(b) H-map



(c) S-map

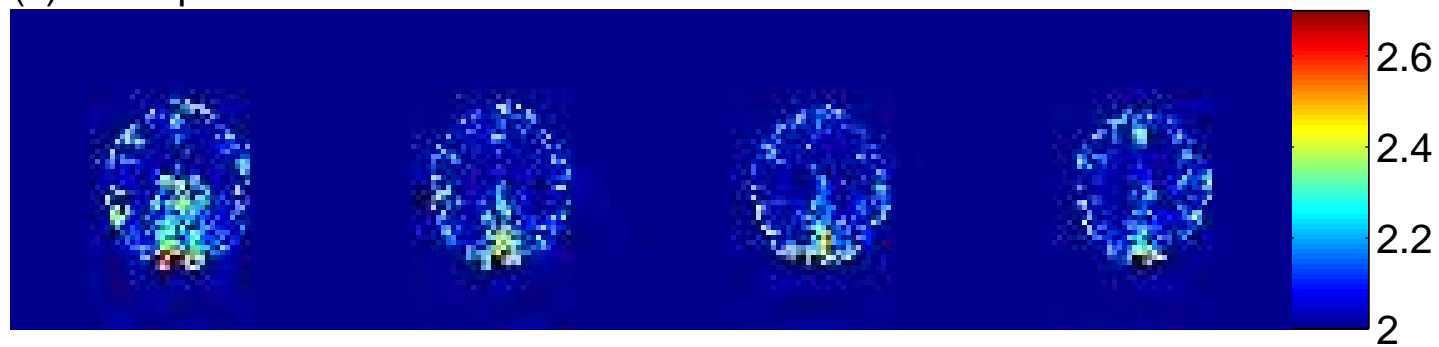
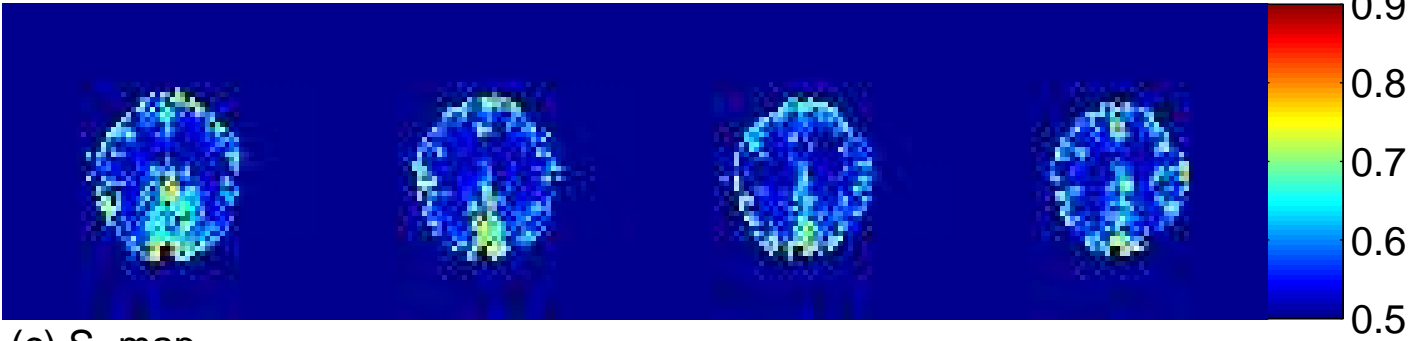


FIG. 2

(a) r-map



(b) H-map



(c) S-map

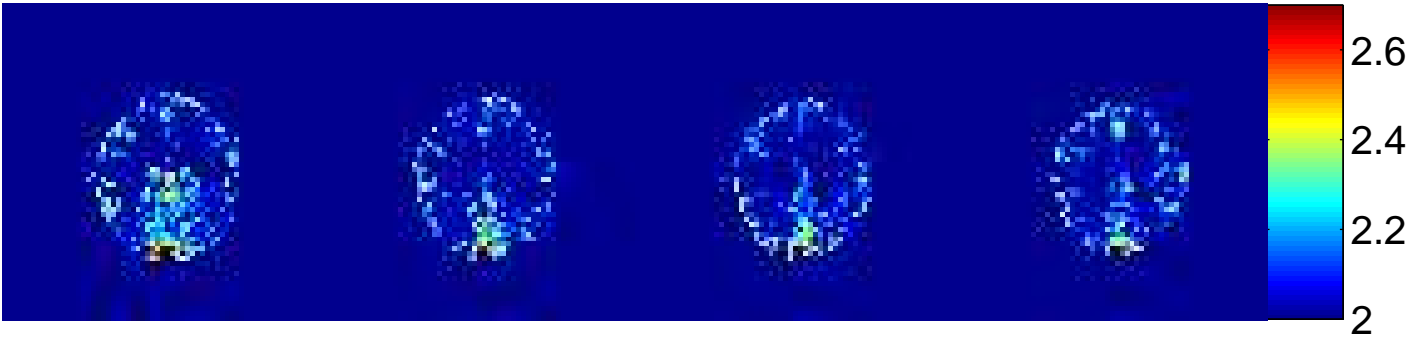


FIG. 3

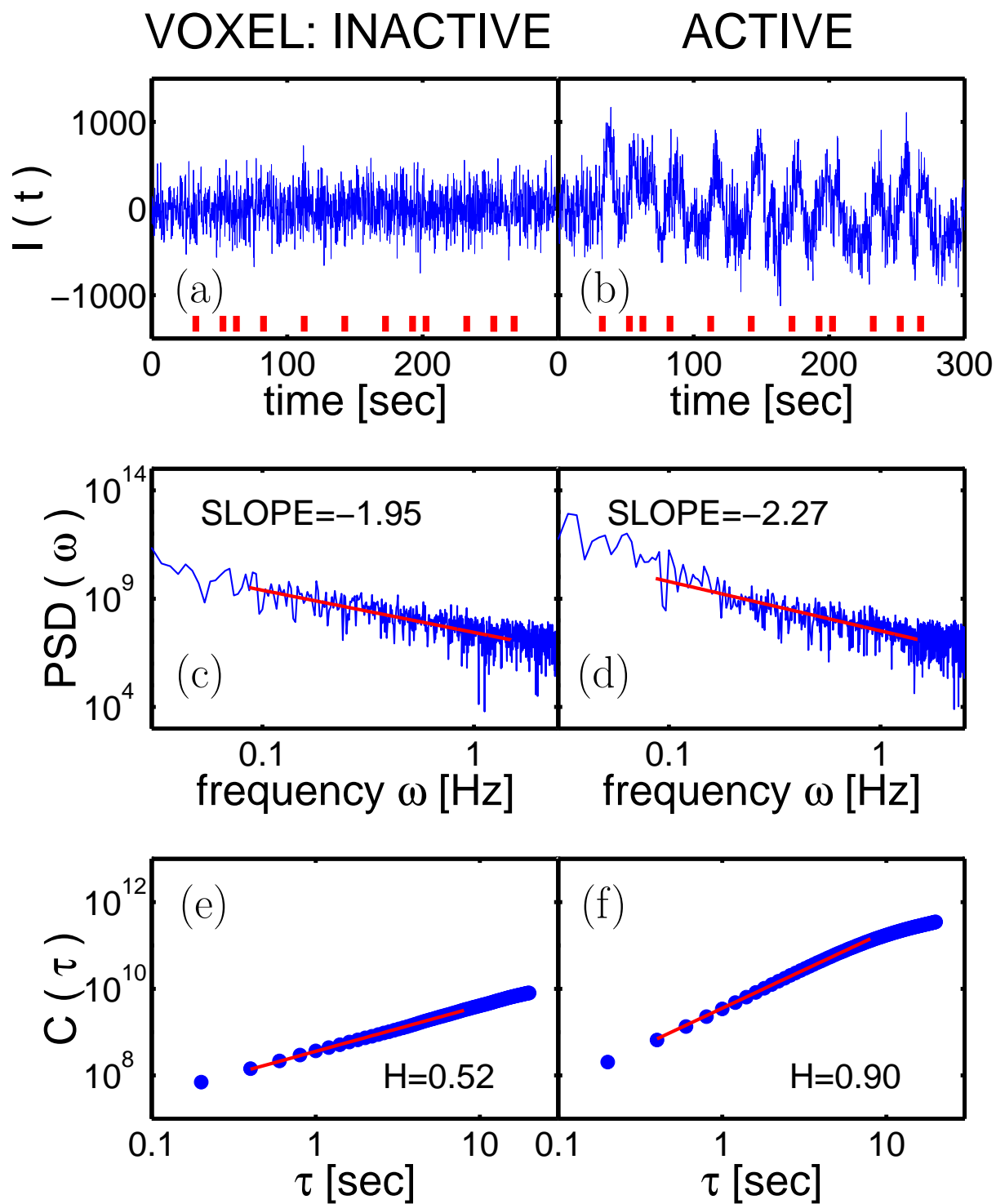


FIG. 4